U–Pb zircon age, geochemical and Sr–Nd isotopic data as constraints on the petrogenesis and emplacement time of andesites from Gerze, southern Qiangtang Block, northern Tibet

Shen Liu [a,b,*], Ruizhong Hu [a], Shan Gao [b], Caixia Feng [a], Ian M. Coulson [c], Guangying Feng [a], Youqiang Qi [a], Yuhong Yang [a], Chaogui Yang [a], Liang Tang [a]

[a] State Key Laboratory of Ore Deposit Geochemistry, Institute of Geochemistry, Chinese Academy of Sciences, Guiyang 550002, China
[b] State Key Laboratory of Geological Processes and Mineral Resources, China University of Geosciences, Wuhan 430074, China
[c] Solid Earth Studies Laboratory, Department of Geology, University of Regina, Regina, Saskatchewan, Canada S4S 0A2

ARTICLE INFO

ABSTRACT

Mesozoic post-collisional andesites occur in the Gerze area within the Qiangtang Terrane of northern Tibet, China. Geochronological, geochemical, and whole-rock Sr–Nd isotopic analyses were performed on this suite of volcanic rocks to characterize their petrogenesis. Laser ablation-inductively coupled plasma-mass spectrometry U–Pb zircon analyses yielded consistent ages ranging from 122.4 ± 0.4 Ma to 124.4 ± 0.4 Ma for two andesite samples (JC01 and GZ01). The andesites belong to the alkaline and sub-alkaline magma series in terms of $K_2O + Na_2O$ contents (4.7–10 wt.%), and belong to the high-K calc-alkaline and calc-alkaline series on the basis of their high K_2O contents (1.0–3.3 wt.%). The volcanic rocks are further characterized by the enrichment of light rare earth elements [$(La/Yb)_N = 7.4–11.5$] and large-ion lithophile elements (e.g., Rb), slightly negative Eu anomalies ($Eu/Eu^* = 0.79–0.94$), and negative anomalies in high field strength elements (e.g., Nb, Ta, and Ti) relative to primitive mantle. The samples show slightly elevated $(^{87}Sr/^{86}Sr)_i$ values that range from 0.7049 to 0.7057, and low $\varepsilon_{Nd}(t)$ values of -3.4 to 0.7. These results suggest that the rocks were derived from a compositionally heterogeneous mantle source and that their parent magmas are basalt magma. The parent mafic magmas may have undergone fractional crystallization of olivine, pyroxene, hornblende, and to a lesser extent, plagioclase during ascent through the thickened crustal pile, with minor or no crustal contamination, before the finally erupting as andesites.

1. Introduction

The Qinghai–Tibet orogenic belt formed via collision between the Asian continent and the Kunlun, Songpan–Ganzi, Qiangtang, Lhasa, and Himalayan Terrenes (Allègre et al., 1984; Chang et al., 1986; Dewey et al., 1988; Yin and Harrison, 2000). Today, the Qiangtang and Lhasa Terrenes are the main components of the plateau (Girardeau et al., 1984, 1985; Dewey et al., 1988; Yin and Harrison, 2000). From the Late Triassic to the Early Jurassic, the Qiangtang Terrane was the site of collisional tectonics characterized by oceanic lithosphere break-off, high- to ultrahigh-pressure metamorphism and denudation, regional-scale extensional tectonics, and magmatism.

A thorough understanding of the occurrence of volcanic rocks in continental orogenic belts, as well as of their origin and source material, is an important component of studies on continental dynamics. Such rocks provide a window into the mantle and aid our understanding of the formative mechanisms of heat–stress anomalies, crust–mantle interaction and material exchange, and geological processes in the deep Earth (Menzies and Pyle, 1990). Therefore, the analyses of the magmatism that occurred during the assembly of individual components of the Qinghai–Tibet Plateau can help reveal the fundamental processes involved in the development of collisional orogens. In this context, the present study seeks to provide insight into Mesozoic magmatism in the Qiangtang Terrane.

In the Mesozoic, various geological processes were simultaneously active in relation to the assembly of the Qinghai–Tibet orogenic belt. It is important, therefore, to distinguish the history of volcanism and tectonism in the Qiangtang Terrane from other processes related to the formation of the Qinghai–Tibet Plateau and from orogenic processes associated with continental collision. Previous studies on the Mesozoic volcanic rocks of the Qinghai–Tibet belt focused on rocks that post-date the collision between the Indian and Asian continents (e.g., Cenozoic potassic volcanic rocks

* Corresponding author at: State Key Laboratory of Ore Deposit Geochemistry, Institute of Geochemistry, Chinese Academy of Sciences, Guiyang 550002, China. Tel.: +86 851 5891962; fax: +86 851 5891664.

E-mail address: liushen@vip.gyig.ac.cn (S. Liu).

at Qiangtang) (Deng, 1989, 1998, 1999; Turner et al., 1996; Ding et al., 1999, 2003, 2007; Miller et al., 1999; Lai and Liu, 2001; Liu et al., 2003, 2008; Williams et al., 2004; Yin et al., 2004; Chi et al., 2005; Chung et al., 2005; Guo et al., 2006; Li et al., 2006, 2007). By contrast, few studies have examined the Mesozoic volcanic rocks in the Qiangtang Terrane (e.g., Bai et al., 2005; Zhu et al., 2006).

In this paper, we present the results of our systematic study of volcanic rocks from Gerze (China), southern Qiangtang Terrane, including new zircon U–Pb age data determined by laser ablation–inductively coupled plasma–mass spectrometry (LA–ICP–MS), whole-rock major and trace element geochemistry, and collection of whole rock Sr–Nd isotopic data. We use this comprehensive dataset to constrain the emplacement age of these volcanic rocks, and discuss their petrogenesis and their significance in the assembly of the Qinghai–Tibet orogenic belt.

2. Geological background and petrology

The study area is located at Gerze, close to the southern margin of the Qiangtang Terrane, northern Tibet, and adjacent to the Banggongco–Nujiang suture zone and Lhasa Terrene (Fig. 1A and B). The volcanic rocks examined in this study occur as expansive lava flows within a continental basin, covering an area of 250–300 km². The exposure of these volcanic rocks is controlled by faults and inferred faults across the basin (Fig. 1B). The volcanic rocks occur in a sequence that includes Jurassic (J1-3) quartz sandstone, limestone, conglomerate, calcareous quartz limestone, calcareous slate, volcanic breccia, andesite, tuff, and dacite; Early Cretaceous (K1) limestone, sandstone, conglomerate, calcareous shale, and volcanic rocks; Kangtog Formation (NK) fuchsia conglomerate, basaltic andesite, andesite, pyroxene andesite, rhyolite, and dacite; and Quaternary (Q) sandstone, conglomerate, quartz sandstone, and laterite. The volcanic rocks are intruded by some diabase dykes. The volcanic units strike approximately E–W (Fig. 1B), similar to the dykes. The studied volcanic rocks are strongly porphyritic (30–50%), dominated by phenocrysts of andesine and labradorite (30–60%; 0.5–2.5 mm long), augite and orthopyroxene (10–25%; 0.8–6.0 mm long), hornblende (2.0–6.0 mm long), and minor biotite (Fig. 2). The groundmass consists of fine-grained (0.06–0.10 mm) plagioclase (altered to aggregates of
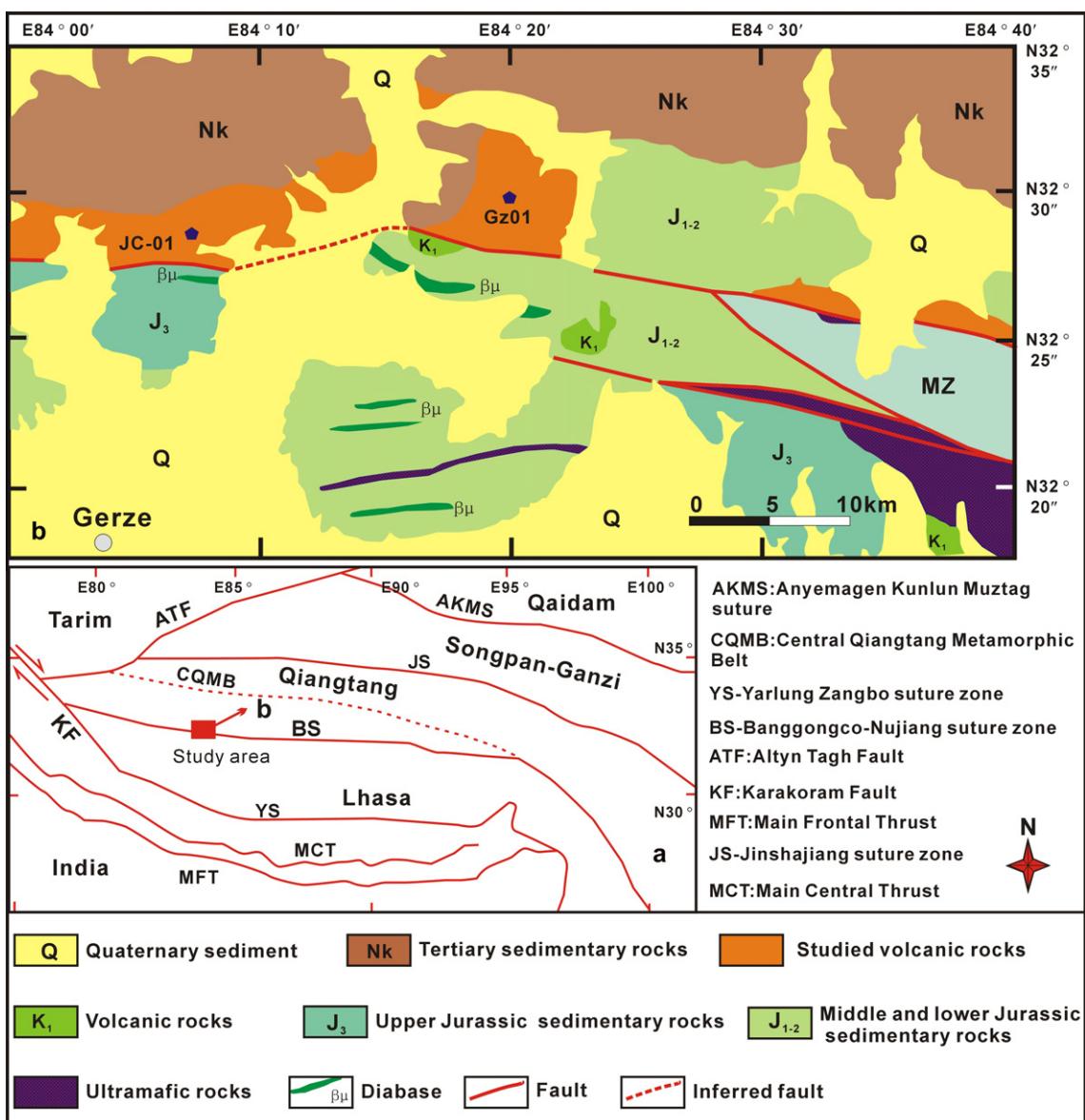

Fig. 1. (a) Simplified tectonic map of Tibet. (b) Geological map of the study area showing the distribution of volcanic rocks across the southern Qiangtang Terrane. Purple pentagons indicate the two sampling sites.
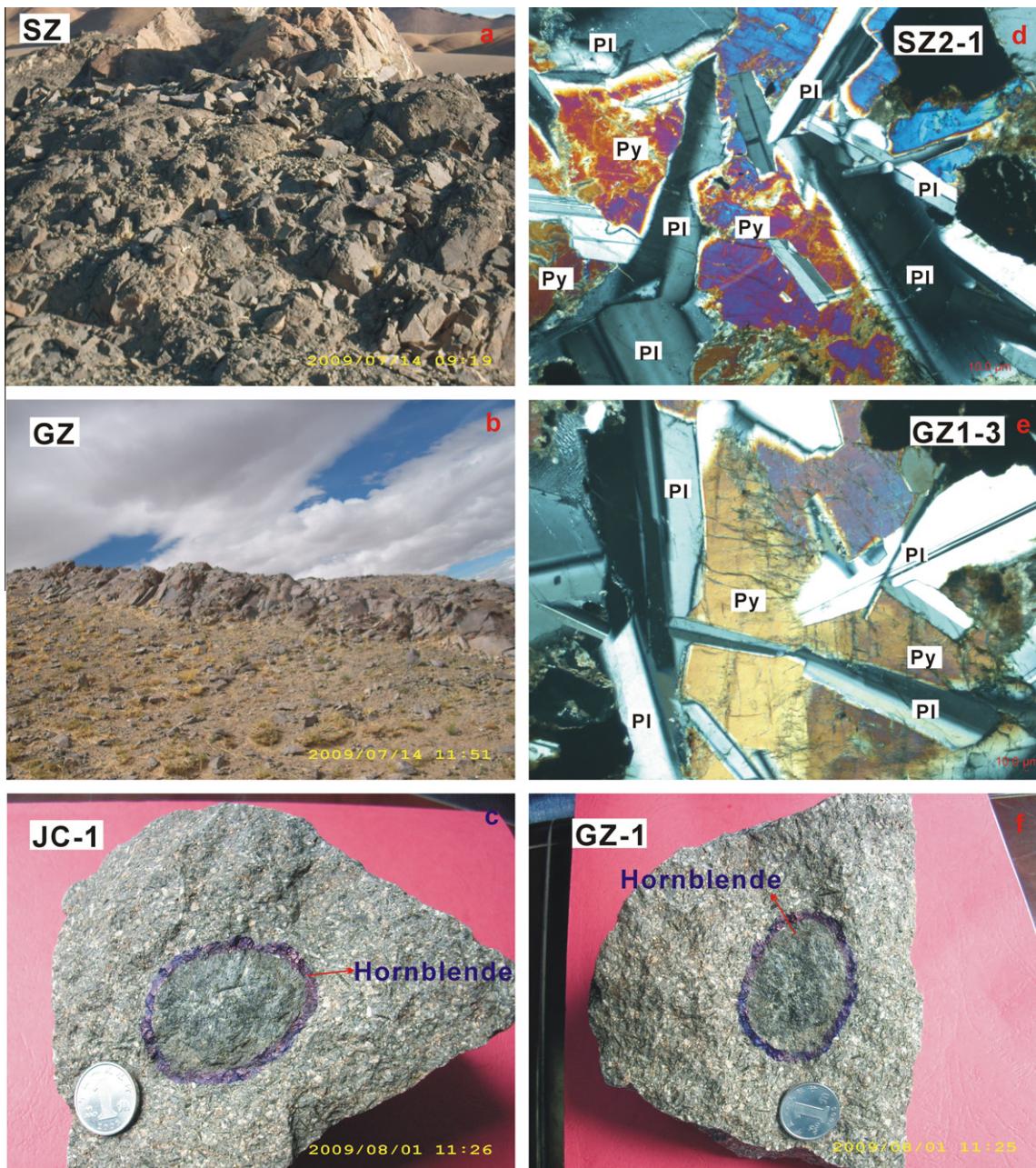
Fig. 2. Representative photographs and photomicrographs showing the petrographic features of volcanic rocks from the Gerze area, southern Qiangtang Terrane, China. The samples are strongly porphyritic, containing phenocrysts of pyroxene, plagioclase, and hornblende.

pargasite, magnesio-hastingsite, and edenite), pyroxene, chlorite, and glass with an andesitic composition. Accessory minerals include zircon, apatite, and magnetite. Petrographically, these rocks are andesite.

3. Analytical methods

3.1. U–Pb dating by LA–ICP–MS

Zircon was separated from two volcanic samples (**JC01** and **GZ01**) using conventional heavy-liquid and magnetic techniques at the Langfang Regional Geological Survey, Hebei Province, China. Zircon separates were examined under transmitted and reflected light, and by cathodoluminescence petrography at the State Key Laboratory of Continental Dynamics, Northwest University, China, to reveal their external and internal structures.

Laser-ablation techniques were employed for zircon age determinations (Table 1; Fig. 3) using an Agilent 7500a ICP–MS instrument equipped with a 193 nm excimer laser, housed at the State Key Laboratory of Geological Processes and Mineral Resources, China University of Geoscience, Wuhan, China. Zircon #91500 was used as a standard and NIST 610 was used to optimize the results. A spot diameter of 24 μm was used. Prior to LA–ICP–MS zircon U–Pb dating, the surfaces of the grain mounts were washed in dilute HNO_3 and pure alcohol to remove potential lead contamination. The analytical methodology is described in detail by Yuan et al. (2004). Correction for common Pb was made following Andersen (2002). Data were processed using the GLITTER and ISOPLOT programs (Ludwig, 2003) (Table 1; Fig. 3). Errors for

Table 1
LA–ICP–MS U–Pb isotopic data for zircon within volcanic rocks from the Gerze area, southern Qiangtang Terrane, China.

| Spot	Th (ppm)	U (ppm)	Pb (ppm)	Th/U	Isotopic ratios						Age (Ma)					
					$^{207}Pb/^{206}Pb$	1σ	$^{207}Pb/^{235}U$	1σ	$^{206}Pb/^{238}U$	1σ	$^{207}Pb/^{206}Pb$	1σ	$^{207}Pb/^{235}U$	1σ	$^{206}Pb/^{238}U$	1σ
JC01																
1	53	108	41.92	0.49	0.1101	0.0015	5.2517	0.074	0.3451	0.0022	1801	17	1861	12	1911	10
2	129	171	3.88	0.75	0.0481	0.0036	0.1261	0.009	0.0190	0.0003	104	166	121	8	121	2
3	267	246	6.07	1.08	0.0461	0.0036	0.1205	0.009	0.0190	0.0003			171	116	8	121	2
4	190	211	4.91	0.90	0.0504	0.0043	0.1323	0.011	0.0190	0.0003	215	193	126	10	121	2
5	412	1350	26.6	0.31	0.0474	0.0013	0.1271	0.004	0.0194	0.0002	70	47	121	3	124	1
6	183	209	4.68	0.87	0.0509	0.0063	0.1323	0.0162	0.0189	0.0003	235	275	126	14	120	2
7	190	1003	19.0	0.19	0.0492	0.0014	0.1315	0.0036	0.0194	0.0002	159	70	125	3	124	1
8	147	1012	18.6	0.15	0.0477	0.0016	0.1269	0.0039	0.0193	0.0002	86	49	121	4	123	2
9	454	384	9.49	1.18	0.0483	0.0026	0.1290	0.0071	0.0194	0.0002	115	102	123	6	124	1
10	254	304	6.48	0.84	0.0555	0.0040	0.1451	0.0111	0.0192	0.0004	431	131	138	10	122	3
11	434	356	8.44	1.22	0.0465	0.0040	0.1153	0.0097	0.0188	0.0003	24	154	111	9	120	2
12	98	770	14.8	0.13	0.0473	0.0047	0.1231	0.0121	0.0189	0.0002	62	216	118	11	121	1
13	299	303	6.85	0.99	0.0491	0.0022	0.1274	0.0060	0.0193	0.0004	154	71	122	5	123	2
14	213	507	10.2	0.42	0.0461	0.0021	0.1226	0.0054	0.0194	0.0002	1.0	74	117	5	124	1
15	354	356	7.84	0.99	0.0571	0.0047	0.1461	0.0135	0.0191	0.0005	497	158	138	12	122	3
GZ01																
1	380	339	8.49	1.12	0.0522	0.0027	0.1381	0.0071	0.0192	0.0002	295	99	131	6	123	1
2	224	238	5.64	0.94	0.0486	0.0023	0.1278	0.0057	0.0193	0.0002	128	79	122	5	123	1
3	403	350	8.71	1.15	0.0484	0.0018	0.1292	0.0048	0.0194	0.0002	119	69	123	4	124	1
4	107	273	99.8	0.39	0.1117	0.0014	5.1790	0.0669	0.3354	0.0020	1828	15	1849	11	1864	10
5	213	429	8.96	0.50	0.0498	0.0021	0.1327	0.0055	0.0195	0.0002	184	78	127	5	124	1
6	329	1112	22.4	0.30	0.0491	0.0011	0.1335	0.0031	0.0197	0.0001	150	41	127	3	126	1
7	138	202	4.57	0.69	0.0496	0.0047	0.1330	0.0125	0.0194	0.0003	177	215	127	11	124	2
8	189	350	7.54	0.54	0.0522	0.0017	0.1424	0.0047	0.0199	0.0002	293	55	135	4	127	1
9	96.0	229	84.9	0.42	0.1140	0.0014	5.3348	0.0725	0.3390	0.0026	1864	14	1874	12	1882	13
10	257	362	8.13	0.71	0.0565	0.0024	0.1527	0.0064	0.0194	0.0003	472	70	144	6	124	2
11	69.9	126	3.29	0.56	0.1370	0.0107	0.3495	0.0272	0.0194	0.0005	2190	98	304	20	124	3
12	262	869	17.2	0.30	0.0461	0.0015	0.1232	0.0037	0.0195	0.000	2	46	118	3	124	1
13	164	1043	19.7	0.16	0.0508	0.0015	0.1358	0.0039	0.0194	0.0002	231	46	129	3	124	1
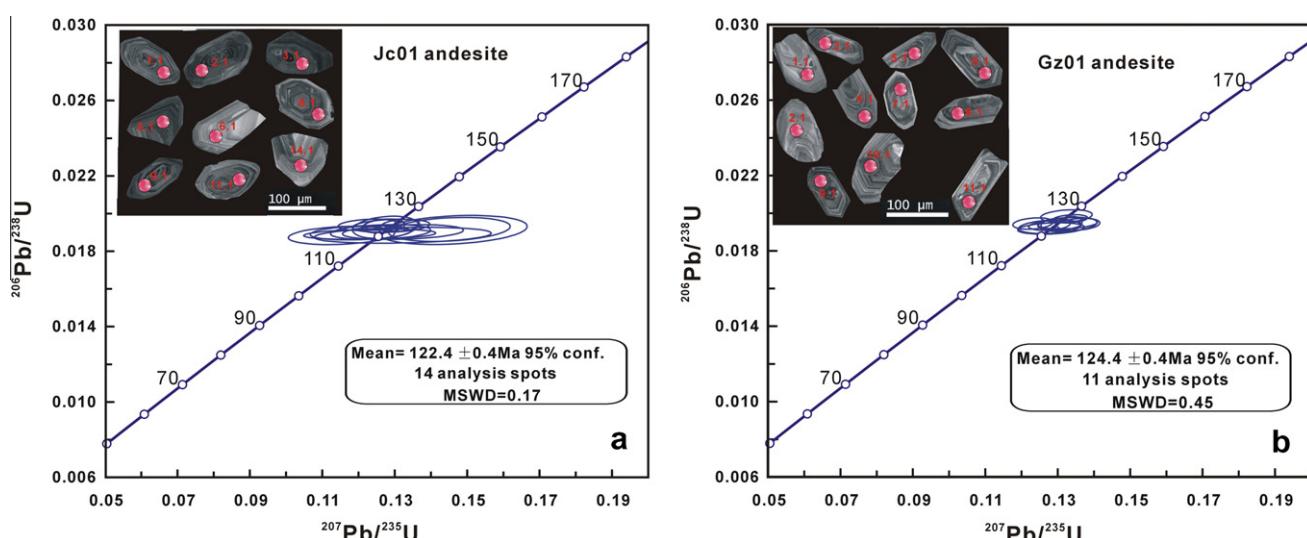
Fig. 3. LA–ICP–MS zircon U–Pb concordia diagrams for volcanic rocks from the Gerze area, southern Qiangtang Terrane, China.

individual analyses by LA–ICP–MS are expressed at the 95% (1σ) confidence level.

3.2. Whole-rock major and trace elements, as well as Sr–Nd isotopes

Forty-seven samples were collected for the analyses of whole-rock major and trace elements, as well as Sr–Nd isotopes. Samples were trimmed to remove altered surfaces, cleaned with deionized water, crushed, and powdered in an agate mill.

Major elements were analyzed with a PANalytical Axios-advance (Axios PW4400) X-ray fluorescence spectrometer at the

State Key Laboratory of Ore Deposit Geochemistry, Institute of Geochemistry, CAS, Guiyang. Fused glass discs were prepared for the analyses of major elements. Analytical precision, as determined for the Chinese National Standards GSR-1 and GSR-3, was better than 5% for all the elements (Table 2). Loss on ignition (LOI) was obtained using 1 g of powder heated to 1100 °C for 1 h.

Trace elements were measured using a Perkin–Elmer Sciex ELAN 6000 ICP–MS at the State Key Laboratory of Ore Deposit Geochemistry, Institute of Geochemistry, CAS. Powdered samples (50 mg) were dissolved in high-pressure Teflon bombs using a HF + HNO₃ mixture and heated for 48 hours at ~190 °C (Qi et al.,

Table 2
Whole-rock major element compositions (wt.%) of representative volcanic rocks from the Gerze area, southern Qiangtang Terrane, China.

Sample	Rock type	SiO$_2$	Al$_2$O$_3$	Fe$_2$O$_3$	MgO	CaO	Na$_2$O	K$_2$O	MnO	P$_2$O$_5$	TiO$_2$	LOI	Total	Mg$^\#$	T (°C)
JC1-2	Andesite	57.03	16.35	6.42	2.57	4.47	5.20	2.01	0.14	0.26	0.63	4.28	99.35	47	745
JC1-3	Andesite	57.27	16.42	6.72	2.73	5.72	4.09	2.01	0.15	0.26	0.63	3.66	99.66	47	745
JC2-1	Andesite	58.48	15.83	6.23	2.22	3.74	4.34	2.97	0.15	0.29	0.83	4.19	99.27	44	802
JC2-5	Andesite	58.36	16.03	7.12	2.67	4.36	3.65	2.92	0.18	0.29	0.83	3.38	99.79	45	814
JC2-8	Andesite	56.80	15.62	6.24	2.26	5.91	4.21	3.13	0.16	0.29	0.82	3.92	99.36	44	779
JC3-1	Andesite	57.87	15.71	6.12	2.93	3.00	4.63	3.13	0.18	0.29	0.82	4.69	99.37	51	800
JC3-2	Andesite	57.88	15.64	6.27	3.33	2.84	4.26	3.04	0.18	0.29	0.82	4.97	99.52	54	807
JC3-3	Andesite	58.46	15.85	6.38	3.41	3.02	4.15	3.11	0.18	0.29	0.82	3.76	99.41	54	809
JC3-4	Andesite	58.29	15.83	6.39	3.39	2.89	4.42	3.16	0.18	0.30	0.82	3.55	99.21	54	804
JC4-1	Andesite	57.68	15.79	6.22	3.16	3.68	5.25	3.20	0.15	0.29	0.82	3.47	99.71	53	792
JC4-2	Andesite	58.49	15.88	6.23	3.00	3.87	4.96	3.06	0.15	0.29	0.81	3.12	99.86	51	803
JC4-3	Andesite	58.07	16.21	6.45	2.51	4.50	4.09	3.16	0.15	0.29	0.84	3.61	99.86	46	809
JC4-5	Andesite	57.59	15.74	6.34	2.55	4.32	4.14	3.16	0.15	0.29	0.82	3.93	99.03	47	804
JC5-1	Andesite	58.44	16.22	6.44	2.38	4.27	4.20	2.84	0.14	0.29	0.85	3.75	99.82	45	817
JC5-2	Andesite	57.62	16.15	6.49	2.38	5.04	3.82	2.79	0.14	0.29	0.83	3.95	99.50	45	810
JC5-3	Andesite	58.49	16.06	6.39	2.33	4.31	4.30	2.81	0.15	0.29	0.84	3.43	99.40	45	809
JC5-5	Andesite	58.09	16.00	6.39	2.41	4.47	4.17	2.80	0.15	0.29	0.83	3.94	99.53	45	814
JC6-1	Andesite	58.39	16.07	6.62	2.37	5.06	3.82	2.71	0.15	0.29	0.84	3.56	99.88	44	811
JC6-2	Andesite	58.11	16.18	6. 50	2.11	5.42	3.93	2.57	0.14	0.30	0.84	3.72	99.81	42	808
JC6-3	Andesite	58.47	16.12	6.54	2.32	5.27	3.42	2.66	0.15	0.29	0.84	3.82	99.89	44	808
JC6-6	Andesite	58.63	16.16	6.35	2.11	5.69	4.17	2.60	0.15	0.29	0.82	2.79	99.76	42	802
JC6-9	Andesite	57.9	16.01	6.07	2.31	4.07	7.04	2.91	0.15	0.29	0.84	2.53	100	46	785
JC7-1	Andesite	58.86	16.09	6.57	2.4	4.92	3.66	2.67	0.17	0.29	0.83	2.97	99.43	46	806
JC7-2	Andesite	58.24	16.3	6.63	2.44	4.07	4.11	2.90	0.15	0.30	0.85	3.85	99.83	49	813
JC7-5	Andesite	58.02	15.83	6.27	2.37	4.60	4.62	3.05	0.13	0.29	0.82	3.53	99.53	48	824
JC7-6	Andesite	57.96	15.84	6.33	2.33	4.63	3.92	3.07	0.15	0.29	0.82	4.36	99.69	45	808
JC8-2	Andesite	58.38	15.82	5.90	2.79	3.40	4.80	2.85	0.14	0.28	0.80	4.26	99.41	51	806
JC8-6	Andesite	58.74	15.85	5.90	1.96	4.25	4.30	2.88	0.15	0.28	0.78	4.22	99.31	42	807
JC9-4	Andesite	58.57	15.97	6.03	2.38	2.87	4.77	3.24	0.13	0.29	0.80	4.14	99.19	46	811
JC10-2	Andesite	57.09	16.32	6.53	2.57	5.73	4.71	1.41	0.13	0.25	0.62	4.13	99.49	46	745
JC10-3	Andesite	56.04	16.31	7.38	2.69	5.35	3.50	2.14	0.16	0.26	0.61	4.86	99.29	45	751
JC10-6	Andesite	57.15	16.14	6.49	2.82	5.55	4.21	2.08	0.15	0.25	0.61	4.15	99.61	49	742
JC12-1	Andesite	57.35	16.22	6.26	2.53	4.19	6.00	1.70	0.14	0.25	0.62	4.23	99.49	47	752
JC12-2	Andesite	57.13	16.39	6.49	2.64	5.15	4.89	2.03	0.14	0.25	0.63	3.58	99.32	47	748
JC12-3	Andesite	57.40	16.49	6.50	2.52	4.24	5.18	2.02	0.14	0.26	0.63	3.81	99.18	46	747
JC12-4	Andesite	57.20	16.41	6.69	2.39	5.61	3.79	2.08	0.14	0.26	0.62	4.21	99.41	44	750
JC12-5	Andesite	57.53	16.43	6.37	2.43	4.37	5.38	1.96	0.14	0.26	0.62	3.96	99.45	46	753
JC12-6	Andesite	57.25	16.34	6.35	2.56	4.40	5.68	2.01	0.13	0.26	0.63	3.82	99.43	47	752
GZ1-1	Andesite	52.29	14.95	8.08	3.58	6.88	3.64	1.30	0.15	0.27	0.99	7.65	99.78	49	741
GZ1-2	Andesite	52.09	15.26	8.24	2.83	7.01	3.95	1.25	0.13	0.28	1.00	7.58	99.62	43	736
GZ1-3	Andesite	51.49	15.30	8.01	2.46	8.23	3.77	0.98	0.15	0.28	1.01	8.12	99.8	40	730
GZ2-2	Andesite	53.03	15.32	7.86	2.27	4.99	7.26	2.12	0.16	0.30	1.03	5.26	99.6	39	729
GZ2-5	Andesite	52.78	15.22	7.80	2.13	4.98	6.65	2.08	0.16	0.30	1.03	6.49	99.61	38	736
GZ3-1	Andesite	56.23	14.11	7.77	2.48	6.36	3.69	1.98	0.23	0.39	0.87	5.28	99.4	41	741
GZ3-3	Andesite	53.25	17.15	8.46	2.66	5.47	5.59	2.15	0.14	0.44	0.96	2.96	99.23	41	772
GZ3-4	Andesite	55.85	14.29	7.86	2.27	7.04	3.86	2.31	0.27	0.39	0.88	4.43	99.46	39	742
GSR-3/R/*		44.64	13.83	13.4	7.77	8.81	3.38	2.32	0.17	0.95	2.37	2.24	99.88		
GSR-3/M/*		44.75	14.14	13.35	7.74	8.82	3.18	2.3	0.16	0.97	2.36	2.12	99.89		
gsr-i/r/*		72.83	13.4	2.14	0.42	1.55	3.13	5.01	0.06	0.09	0.29	0.7	99.62		
GSR-1/W		72.65	13.52	2.18	0.46	1.56	3.15	5.03	0.06	0.11	0.29	0.69	99.7		

LOI: loss on ignition. Mg$^\#$ = 100 ∗ Mg/(Mg + $\sum$Fe) atomic ratio. RV*: recommended values; MV*: measured values; values for GSR-1 and GSR-3 are from Wang et al. (2003).

2000). Rh was used as an internal standard to monitor signal drift during counting. The analyses of the international standard GBPG-1 indicated a precision generally better than 5% for all elements. The analyses of the international standards OU-6 and GBPG-1 are in close agreement (≤8.0%) with recommended values (Table 3).

For the analyses of Rb–Sr and Sm–Nd isotopes, sample powders were spiked with mixed isotope tracers, dissolved in Teflon capsules with HF + HNO$_3$ acids, and separated by conventional cation-exchange techniques. Isotopic measurements were performed on a Finnigan Triton Ti thermal ionization mass spectrometer at the State Key Laboratory of Geological Processes and Mineral Resources, China University of Geosciences, Wuhan, China. Procedural blanks were <200 pg for Sm and Nd, and <500 pg for Rb and Sr. Mass fractionation corrections for Sr and Nd isotopic ratios were based on ^{86}Sr/^{88}Sr = 0.1194 and ^{146}Nd/^{144}Nd = 0.7219, respectively. The analyses of standards during the period of analysis yield the following results: NBS987 gives ^{87}Sr/^{86}Sr = 0.710246 ± 16 (2σ)

and La Jolla yields ^{143}Nd/^{144}Nd = 0.511863 ± 8 (2σ). The analytical results for Sr–Nd isotopes are presented in Table 4.

4. Results

4.1. LA–ICP–MS U–Pb age determination

Euhedral zircon grains in samples JC01 and GZ01 are clean and prismatic, with magmatic oscillatory zoning. Apart from three analyses that provided significantly older ages (JC01, spot 1; GZ01, spots 4 and 9), 14 grains yield a weighted mean ^{206}Pb/^{238}U age of 122.4 ± 0.42 Ma (2σ) (95% confidence interval) for JC01 (Table 1; Fig. 3a), and 11 grains give a weighted mean ^{206}Pb/^{238}U age of 124.4 ± 0.38 Ma (2σ) (95% confidence interval) for GZ01 (Table 1; Fig. 3b). These determinations are the best estimates of the crystallization ages of samples JC01 and GZ01. The rejected

Table 3
Trace element contents (ppm) of representative volcanic rocks from the Gerze area, southern Qiangtang Terrane, China.

Sample	OU-6(RV*)	GBPG-1(RV*)	OU-6(MV*)	GBPG-1(MV*)	JC1-2	JC1-3	JC2-1	JC2-5	JC2-8	JC3-1	JC3-2	JC3-3	JC3-4	JC4-1	JC4-2	JC4-3	JC4-5	JC5-1	JC5-2	JC5-3	JC5-5	JC6-1	JC6-2	JC6-3
Sc	22..1	13.9	23.0	13.8	12.7	12.5	13.0	13.1	12.3	13.2	13.2	13.3	13.6	13.4	14.9	15.4	14.9	15.0	15.0	15.2	15.6	15.0	15.4	15.0
V	129	96.5	123	96.0	136	142	135	132	132	131	129	128	132	132	147	148	147	149	153	149	160	149	152	147
Cr	70.8	181	70.5	179	14.5	14.5	9.2	8.9	8.0	8.4	9.7	9.4	8.7	11.9	9.6	9.1	9.2	15.5	9.8	9.7	10.6	10.3	9.8	
Co	29.1	19.5	28.2	19.8	34.4	27.4	49.4	33.8	30.1	23.4	20.9	20.2	19.6	25.7	26.7	30.7	26.2	29.1	27.4	26.3	26.9	37.6	39.3	37.9
Ni	39.8	59.6	40.0	57.2	6.56	6.68	2.42	3.05	2.53	2.38	3.55	1.68	1.91	2.95	4.64	2.15	2.52	2.45	6.14	2.86	2.34	3.33	2.91	3.45
Cu	39.6	30.0	43.7	28.7	37.7	39.5	11.8	12.2	10.8	12.6	12.2	11.1	12.8	11.6	10.7	11.4	10.6	11.3	11.7	14.1	10.9	11.8	11.7	10.7
Zn	111	80.3	111.0	76.6	128	130	163	167	161	169	155	159	162	153	134	137	127	135	140	127	133	141	150	126
Ga	24.3	18.6	24.1	19.2	14.5	15.8	17.3	17.7	17.9	16.8	16.6	16.9	17.0	17.1	18.6	18.8	17.9	19.4	18.9	19.2	19.9	19.8	19.8	19.7
Rb	120	56.2	117	57.5	49.4	50.8	64.4	70.6	86.3	74.3	74.8	80.9	79.9	73.5	80.5	76.1	73.8	74.2	71.9	75.8	72.0	76.3	72.6	
Sr	131	364	128	365	1292	895	1018	897	812	886	780	772	762	1000	926	1116	1208	1270	1123	1301	1302	1042	991	985
Y	27.4	18.0	27.2	19.3	14.6	14.9	21.2	22.9	21.3	21.5	22.1	21.5	21.0	21.8	23.0	24.3	23.3	23.6	23.6	24.5	24.5	24.3	24.9	24.9
Zr	174	232	169	251	84.5	84.8	150	170	151	144	147	150	145	150	165	170	166	179	176	168	180	176	176	166
Nb	14.8	9.9	14.7	10.1	5.8	6.0	13.5	12.4	13.3	11.7	11.7	11.9	12.2	12.1	12.2	12.8	11.8	12.0	13.7	12.1	15.5	12.2	12.8	12.0
Cs	8.02	0.32	8.14	0.33	1.88	1.91	3.84	3.37	3.81	3.19	3.34	3.78	3.79	2.47	3.11	2.66	2.08	2.63	2.05	2.53	2.60	2.11	2.69	2.31
Ba	477	908	480	915	437	524	757	846	772	1663	1446	1241	1158	1106	865	977	832	587	582	591	603	623	629	596
La	33.0	53.0	32.6	54.0	18.2	22.5	33.6	32.4	32.9	31.3	30.7	30.6	30.4	32.7	33.6	35.2	34.9	34.8	33.9	35.4	36.7	37.0	36.5	37.4
Ce	74.4	103.2	79.1	94.7	38.7	44.3	71.2	68.6	68.2	67.9	65.0	62.5	63.9	67.7	63.3	66.3	65.0	67.2	65.5	66.1	69.2	69.1	69.2	69.6
Pr	7.80	11.5	7.71	12.0	4.32	4.68	7.58	7.56	7.46	7.62	7.12	6.84	6.97	7.43	7.61	8.03	7.71	8.01	7.91	8.02	8.30	8.34	8.51	8.39
Nd	29.0	43.3	29.9	44.2	16.6	17.9	28.8	29.0	28.5	28.4	27.0	25.8	26.7	28.7	28.4	30.1	28.8	30.4	29.9	30.8	30.4	31.1	31.6	31.6
Sm	5.92	6.79	5.79	7.06	3.35	3.57	5.64	5.82	5.59	5.44	5.31	5.19	5.63	5.38	5.73	5.53	5.70	5.66	5.87	5.99	6.06	6.16	6.14	
Eu	1.36	1.79	1.34	1.82	0.98	1.03	1.37	1.58	1.42	1.49	1.38	1.46	1.31	1.48	1.39	1.52	1.49	1.52	1.44	1.50	1.51	1.57	1.60	1.56
Gd	5.27	4.74	5.20	4.89	3.08	3.34	5.05	5.45	5.07	5.38	5.22	5.21	4.93	5.44	5.13	5.53	5.15	5.33	5.12	5.22	5.41	5.37	5.47	5.65
Tb	0.85	0.60	0.84	0.65	0.46	0.48	0.71	0.78	0.72	0.74	0.73	0.71	0.70	0.70	0.75	0.78	0.76	0.76	0.76	0.80	0.81	0.78	0.83	0.82
Dy	4.99	3.26	4.98	3.33	2.49	2.58	3.69	4.11	3.82	3.82	3.94	3.85	3.71	3.87	3.96	4.17	3.99	4.05	4.03	4.09	4.22	4.23	4.23	4.25
Ho	1.01	0.69	1.04	0.67	0.49	0.49	0.73	0.78	0.74	0.77	0.77	0.73	0.71	0.74	0.77	0.81	0.79	0.80	0.80	0.84	0.83	0.86	0.86	0.83
Er	2.98	2.01	2.97	2.08	1.56	1.61	2.29	2.41	2.24	2.31	2.47	2.24	2.35	2.28	2.37	2.45	2.45	2.49	2.48	2.48	2.59	2.59	2.48	2.54
Tm	0.44	0.30	0.43	0.31	0.22	0.22	0.33	0.34	0.31	0.33	0.32	0.32	0.32	0.32	0.34	0.35	0.34	0.35	0.34	0.33	0.34	0.34	0.35	0.34
Yb	3.00	2.03	2.97	2.11	1.55	1.62	2.24	2.39	2.27	2.28	2.36	2.29	2.18	2.28	2.21	2.39	2.29	2.32	2.35	2.27	2.41	2.38	2.47	2.38
Lu	0.45	0.31	0.45	0.32	0.23	0.23	0.35	0.34	0.33	0.32	0.35	0.31	0.32	0.33	0.32	0.35	0.33	0.34	0.33	0.34	0.36	0.35	0.35	0.33
Hf	4.70	6.07	4.68	6.12	2.15	2.33	4.32	4.67	4.30	4.15	4.16	4.30	4.19	4.09	3.89	3.96	3.90	4.25	4.11	4.08	4.23	4.24	4.26	3.92
Ta	1.06	0.40	1.11	0.42	0.42	0.42	1.36	0.90	1.03	0.93	0.86	0.92	0.87	0.91	0.86	0.85	0.89	0.83	1.06	0.82	1.11	0.82	0.87	0.82
Pb	28.2	14.1	32.3	13.4	18.2	18.6	19.6	24.6	21.8	25.2	21.8	23.1	21.5	18.8	22.1	19.5	17.6	28.7	23.5	18.9	20.7	17.3	18.3	19.4
Th	11.5	11.2	11.2	12.0	4.63	4.96	9.63	9.81	9.69	9.37	9.58	9.36	9.46	9.58	10.0	10.2	9.9	10.2	10.4	10.0	10.4	10.7	10.7	10.5
U	1.96	0.90	1.97	0.91	1.23	1.31	2.36	2.03	2.31	2.41	2.31	2.29	2.19	2.15	1.98	2.20	1.88	2.18	2.21	2.16	2.24	2.35	2.35	2.23
δEu					0.93	0.91	0.78	0.86	0.81	0.84	0.80	0.86	0.80	0.81	0.81	0.82	0.86	0.84	0.82	0.83	0.81	0.84	0.84	0.81

	JC6-6	JC6-9	JC7-1	JC7-2	JC7-5	JC7-6	JC8-2	JC8-6	JC9-4	JC10-2	JC10-3	JC10-6	JC12-1	JC12-2	JC12-3	JC12-4	JC12-J	JC12-6	GZ1-1	GZ1-2	GZ1-3	GZ2-2	GZ2-5	GZ3-1	GZ3-3	GZ3-4
Sc	14.2	15.0	14.7	15.1	18.8	15.3	13.5	13.5	14.1	13.5	13.1	12.4	14.4	13.8	13.3	13.4	14.4	15.2	19.5	18.8	18.9	20.9	21.5	14.8	19.4	17.0
V	143	155	144	154	198	157	137	133	143	151	146	146	158	152	143	155	153	158	204	145	204	89	83	174	207	185
Cr	13.6	9.9	13.4	11.1	13.1	10.8	8.4	9.7	10.9	17.4	15.3	14.6	17.9	17.6	20.1	16.3	16.0	18.6	44.4	47.6	42.5	48.9	61.3	7.2	8.0	8.9
Co	37.4	32.3	41.7	32.0	54.3	40.3	20.9	33.0	25.1	31.2	31.0	32.9	32.9	34.5	39.5	35.2	34.4	31.1	28.5	27.2	35.1	48.6	35.6	32.2	43.8	
Ni	2.94	4.60	5.99	2.68	4.90	3.03	3.01	3.36	2.64	8.86	8.56	8.47	8.35	9.49	11.69	8.70	7.97	8.76	18.9	20.5	19	18.2	23	6.4	5.5	6.2
Cu	13.4	12.0	12.2	11.8	14.3	10.8	10.8	9.8	10.5	34.8	35.3	33.3	35.1	35.9	34.6	38.0	34.8	37.1	28.8	31.1	33.7	16.4	18.9	27.0	48.5	34.3
Zn	148	135	136	137	168	152	143	117	138	107	99.4	102	110	107	106	108	110	107	126	132	126	118	119	115	150	119
Ga	19.4	19.7	19.7	19.7	24.1	19.2	18.8	18.7	17.8	15.3	17.2	16.6	15.8	16.1	14.7	16.5	16.5	15.6	17.5	18.0	17.2	16.0	15.9	16.9	18.6	16.4
Rb	76.2	74.5	67.2	78.8	109.6	95.8	72.4	73.7	71.1	28.7	53.2	48.8	39.9	52.0	44.3	50.1	45.0	49.3	32.3	31.6	24.7	45.9	48.7	41.8	51.5	62.7
Sr	916	1368	1121	1282	1437	1174	1213	1166	1303	1042	908	841	1518	1093	1332	1080	1450	1405	431	395	443	499	504	698	1204	708
Y	24.9	25.0	24.6	24.8	29.7	24.0	23.3	22.5	23.0	14.9	15.5	15.1	15.5	15.5	14.9	15.3	16.0	15.7	20.3	18.5	20	21.5	21.1	20.5	24.7	22.2
Zr	172	164	160	167	216	172	158	165	160	88	87	84	93.8	90.1	82.9	87.6	91.8	94.7	105	99.8	104	106	110	102	138	116
Nb	12.3	11.6	11.2	12.3	15.5	12.6	11.2	12.0	11.7	5.58	5.37	4.89	5.74	5.67	4.95	5.29	5.62	5.92	7.40	7.22	7.80	7.79	8.18	6.56	9.71	7.93
Cs	2.65	2.19	1.99	2.04	2.87	2.31	1.53	2.41	1.50	2.07	2.07	1.84	1.52	1.84	1.67	1.65	1.72	1.85	0.88	1.00	1.07	0.50	0.51	1.25	0.82	1.52
Ba	580	629	590	620	826	609	678	619	666	421	572	541	381	500	455	572	485	477	260	317	159	380	392	390	444	435
La	36.4	37.1	35.8	37.5	45.4	35.2	34.1	35.8	35.2	19.3	20.3	20.4	21.4	19.6	19.3	19.8	21.0	21.1	20.1	20.4	19.8	20.6	19.9	27.4	30.3	26.1
Ce	67.7	69.8	68.0	69.4	85.4	67.1	64.0	67.1	66.0	36.2	37.1	37.1	39.5	37.8	36.5	37.8	39.3	38.7	39.8	39.9	40	40.5	38.7	54.9	60.1	51.4

Pr	8.28	8.42	8.09	8.37	10.0	7.99	7.72	7.79	7.79	4.33	4.36	4.45	4.74	4.66	4.34	4.57	4.68	4.57	5.01	4.92	4.96	5.21	5.12	6.73	7.47	6.46
Nd	30.4	31.2	30.5	31.6	37.7	30.1	28.8	29.8	29.9	17.1	17.7	17.7	18.3	17.9	16.9	17.8	18.5	17.7	20.4	19.9	20.4	21.4	20.8	26.4	30.3	26.1
Sm	5.82	6.01	5.97	5.95	7.30	5.85	5.53	5.78	5.76	3.53	3.65	3.55	3.70	3.59	3.46	3.67	3.62	3.64	4.11	3.96	4.09	4.62	4.41	5.18	5.71	5.29
Eu	1.56	1.59	1.54	1.57	1.86	1.50	1.37	1.45	1.53	1.00	0.99	1.07	1.07	1.08	0.99	1.06	1.10	1.00	1.21	1.16	1.2	1.25	1.28	1.45	1.63	1.46
Gd	5.58	5.30	5.23	5.39	6.60	5.20	5.06	5.18	5.35	3.26	3.40	3.41	3.42	3.45	3.38	3.47	3.67	3.47	4.11	3.99	4.15	4.44	4.3	4.71	5.32	4.78
Tb	0.79	0.82	0.79	0.81	0.97	0.80	0.74	0.75	0.79	0.46	0.48	0.47	0.50	0.51	0.49	0.49	0.49	0.47	0.63	0.6	0.63	0.65	0.66	0.69	0.80	0.71
Dy	4.27	4.41	4.15	4.18	5.03	4.05	3.99	4.01	4.24	2.60	2.70	2.55	2.69	2.67	2.53	2.70	2.72	2.69	3.48	3.42	3.5	3.57	3.56	3.5	4.25	3.73
Ho	0.86	0.85	0.82	0.81	1.01	0.79	0.79	0.74	0.79	0.50	0.51	0.49	0.52	0.51	0.49	0.51	0.53	0.51	0.65	0.65	0.67	0.72	0.69	0.68	0.80	0.72
Er	2.50	2.56	2.54	2.48	3.06	2.47	2.39	2.33	2.36	1.55	1.59	1.57	1.61	1.59	1.52	1.58	1.66	1.57	2.04	1.98	2.05	2.16	2.08	2.12	2.63	2.23
Tm	0.34	0.37	0.35	0.34	0.42	0.32	0.33	0.33	0.32	0.21	0.23	0.22	0.23	0.22	0.21	0.22	0.22	0.21	0.27	0.28	0.27	0.29	0.29	0.28	0.33	0.31
Yb	2.27	2.35	2.32	2.34	2.95	2.29	2.27	2.32	2.27	1.57	1.63	1.58	1.54	1.54	1.46	1.54	1.62	1.52	1.91	1.89	1.93	1.94	1.88	1.95	2.43	2.10
Lu	0.35	0.34	0.34	0.35	0.45	0.34	0.32	0.34	0.35	0.23	0.24	0.23	0.24	0.24	0.22	0.24	0.24	0.24	0.27	0.26	0.28	0.29	0.27	0.28	0.35	0.29
Hf	3.92	3.81	3.82	3.79	4.95	4.12	3.77	3.95	3.75	2.09	1.96	1.94	2.09	2.09	1.83	1.98	2.09	2.04	2.44	2.15	2.39	2.46	2.64	2.27	3.04	2.55
Ta	0.81	0.88	0.81	0.92	1.05	0.76	0.83	0.84	0.79	0.37	0.34	0.31	0.37	0.37	0.33	0.34	0.38	0.37	0.48	0.45	0.5	0.5	0.53	0.39	0.73	0.47
Pb	23.4	20.4	20.1	19.3	29.4	22.1	21.6	17.5	23.8	15.7	17.8	17.3	17.6	17.6	17.5	16.4	17.9	44.8	13.3	12.5	13.4	17	16.4	14.8	16.9	14.6
Th	10.5	10.1	10.1	10.4	13.1	10.1	10.2	10.0	9.95	4.61	4.79	4.73	4.86	4.68	4.48	4.77	4.71	4.78	4.89	4.92	4.82	4.75	4.86	5.39	6.25	5.32
U	2.23	2.28	2.17	2.10	2.69	1.87	2.07	2.29	1.92	1.21	1.25	1.19	1.29	1.24	1.15	1.21	1.25	1.28	1.13	1.16	1.13	0.82	0.81	0.86	1.44	0.90
δEu	0.84	0.86	0.84	0.85	0.82	0.83	0.79	0.81	0.84	0.90	0.86	0.94	0.92	0.94	0.88	0.91	0.92	0.86	0.90	0.89	0.89	0.84	0.90	0.90	0.90	0.89

RV*: recommended values; MV*: measured values. Values for GBPG-1 are from Thompson et al. (2000); those for OU-6 are from Potts and Kane (2005).

Table 4
Sr–Nd isotopic compositions for volcanic rocks from the Gerze area, southern Qiangtang Terrane, China.

| 样品号	Sm (ppm)	Nd (ppm)	Rb (ppm)	Sr (ppm)	$^{87}Rb/^{86}Sr$	$^{87}Sr/^{86}Sr$	2σ-m	$(^{87}Sr/^{86}Sr)$	$^{147}Stn/^{144}Nd$	$^{143}Nd/^{144}Nd$	2σ-m	$(^{143}Nd/^{144}Nd)i$	$\varepsilon_{Nd}(t)$
JC1-2	3.35	16.6	49.4	1292	0.111	0.705670	13	0.705478	0.1221	0.512498	9	0.512400	−1.6
JC2-5	5.57	28.5	59.5	923	0.186	0.705890	14	0.705566	0.1181	0.512401	9	0.512306	−3.4
JC3-1	5.44	28.4	74.3	886	0.242	0.706095	14	0.705674	0.1157	0.512419	8	0.512327	−3.0
JC3-3	5.19	25.8	80.9	772	0.303	0.706087	11	0.705559	0.1217	0.512492	9	0.512395	−1.7
JC4-5	5.53	28.8	73.6	1208	0.176	0.705962	14	0.705656	0.1160	0.512506	9	0.512413	−1.3
JC5-1	5.70	30.4	73.8	1270	0.168	0.705911	13	0.705619	0.1134	0.512521	9	0.512430	−1.0
JC5-5	5.99	30.4	75.8	1302	0.168	0.705926	14	0.705634	0.1191	0.512520	9	0.512425	−1.1
JC6-1	6.06	31.1	72.0	1042	0.200	0.705826	11	0.705479	0.1176	0.512456	10	0.512362	−2.3
JC6-5	6.02	31.6	81.3	975	0.241	0.705697	16	0.705278	0.1153	0.512443	10	0.512351	−2.5
JC7-2	5.95	31.6	78.8	1282	0.178	0.705911	16	0.705602	0.1140	0.512438	9	0.512347	−2.6
JC8-2	5.53	28.8	72.4	1213	0.173	0.705875	11	0.705575	0.1160	0.512439	9	0.512346	−2.6
JC9-4	5.76	29.9	71.1	1303	0.158	0.705866	14	0.705591	0.1165	0.512446	9	0.512353	−2.5
JC10-2	3.53	17.1	28.7	1042	0.080	0.705394	14	0.705255	0.1249	0.512577	9	0.512477	−0.1
JC12-5	3.62	18.5	45.0	1450	0.090	0.705685	14	0.705529	0.1186	0.512577	12	0.512482	0.03
GZ1-1	4.11	20.4	32.3	431	0.216	0.705474	16	0.705091	0.1220	0.512576	12	0.512477	0.0
GZ1-2	3.96	19.9	31.6	395	0.231	0.705365	16	0.704957	0.1202	0.512579	10	0.512482	0.1
GZ2-1	4.24	20.6	95.2	517	0.532	0.705995	14	0.705054	0.1242	0.512541	10	0.512440	−0.7
GZ2-5	4.41	20.8	48.7	504	0.279	0.705615	16	0.705121	0.1280	0.512552	12	0.512447	−0.6
GZ3-1	5.18	26.4	41.8	698	0.173	0.705295	11	0.704989	0.1186	0.512609	10	0.512513	0.7
GZ3-4	5.60	29.2	52.3	824	0.183	0.705346	14	0.705022	0.1159	0.512597	9	0.512503	0.5

2σ-m: 2 sigma-mean.
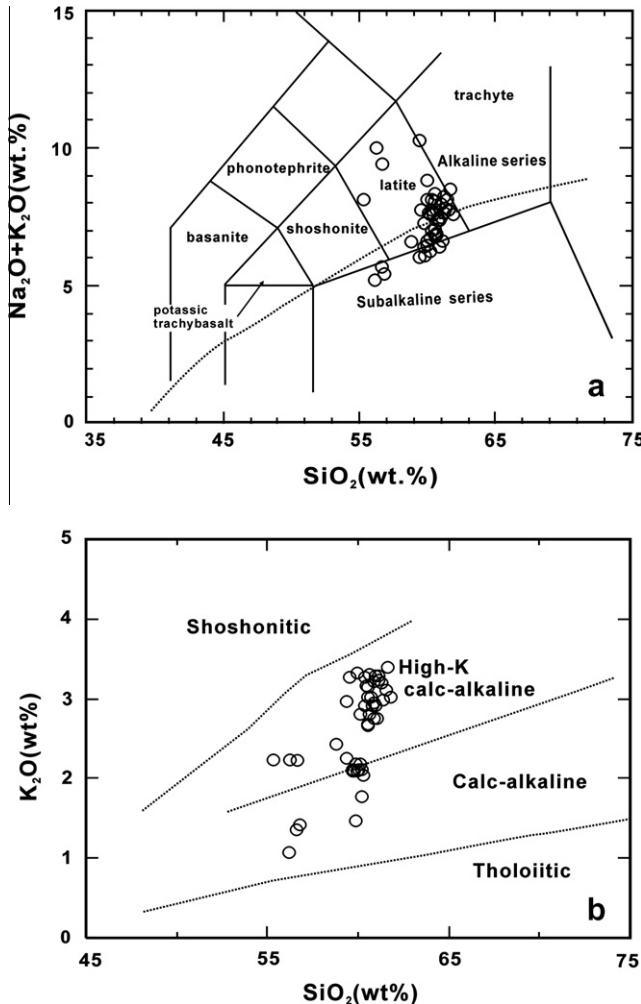
Fig. 4. SiO$_2$ versus: (a) Na$_2$O + K$_2$O and (b) K$_2$O for volcanic rocks from the Gerze area, southern Qiangtang Terrane, China.

analyses, which yield ^{206}Pb/^{238}U ages of 1911 Ma (JC01, spot 1), 1864 Ma (GZ01, spot 4), and 1882 Ma (GZ01, spot 9), are interpreted to represent inherited zircons.

4.2. Major and trace elements

Tables 2 and 3 show representative whole-rock major and trace element data for the studied andesites, which have low to moderate

SiO$_2$ contents (56–59 wt.%) and MgO contents (1.2–3.0 wt.%), Mg$^{\#}$ = 38–54, relatively high Na$_2$O contents (3.5–7.3 wt.%), and variable K$_2$O contents (0.9–3.2 wt.%) (Table 2). In a plot of alkalis versus SiO$_2$ (Fig. 4a), the samples plot in the fields for the alkaline and sub-alkaline series. In a plot of K$_2$O versus SiO$_2$ (Fig. 4b), the samples plot in the calc-alkaline and high-K calc-alkaline fields. The samples have variable contents of Al$_2$O$_3$ (14.1–17.2 wt.%), Fe$_2$O$_3$ (5.9–8.5 wt.%), and CaO (2.8–8.2 wt.%), as well as uniformly low contents of TiO$_2$ (0.6–1.0 wt.%) and P$_2$O$_5$ (0.2–0.4 wt.%).

All of the samples show highly variable contents of Sr (395–1450 ppm) and Ba (159–1663 ppm), are enriched in light rare earth elements (LREEs; e.g., (La/Yb)$_N$ = 7.4–11.5), and have slightly negative Eu anomalies (δEu = 0.79–0.94) (Table 3; Fig. 5a). In a primitive mantle-normalized trace elemental diagram, the volcanic rocks are characterized by enrichment in Rb, U, La, Pb, Sr, and Zr, as well as depletion in Ba and high field strength elements (HFSEs; Ta, Nb, Hf, and Ti) (Fig. 5b). The enrichment in Zr possibly reflects the abundance of zircon. The andesites show regular trends of decreasing MgO, Fe$_2$O$_3$, CaO, TiO$_2$, Cr, and Ni with increasing SiO$_2$ (Figs. 6a, c, d, e, and 7e and f), and weak correlations between K$_2$O, P$_2$O$_5$, Ba, Rb, Sr, Zr, and SiO$_2$ (Figs. 6g, h, 7a–d). There is no apparent correlation between SiO$_2$ and each of Al$_2$O$_3$ or Na$_2$O (Fig. 6b, f).

4.3. Sr–Nd isotopes

Sr and Nd isotopic data for representative samples of the volcanic rocks (Table 4; Fig. 8) yield moderate ranges in (^{87}Sr/^{86}Sr)$_i$ values (0.7049–0.7057) and initial $\varepsilon_{Nd}(t)$ values (−3.4 to 0.7). The Sr–Nd isotopes of the studied samples overlap with those of the Qiangtang Cenozoic potassic volcanic rocks (Liu et al., 2008).

5. Petrogenesis

5.1. Crustal contamination

Generally, there is an agreement that these magmas experienced some degree of crustal contamination during ascent and/or residence within crustal magma chambers. It is necessary, therefore, to evaluate the extent of crustal contamination. Geochemical characteristics, including significant depletion in Nb–Ta, relatively high Sr isotopic composition and negative $\varepsilon_{Nd}(t)$, suggest a role of a continental component in the magma genesis of the andesites. Crustal assimilation can cause significant variations in Sr–Nd isotopes within a group of rocks, and produces a negative correlation between SiO$_2$ and $\varepsilon_{Nd}(t)$ values, as well as a positive correlation between SiO$_2$ and (^{87}Sr/^{86}Sr)$_i$ values. These features are not observed in the studied volcanic rocks from Gerze, indicating a general lack
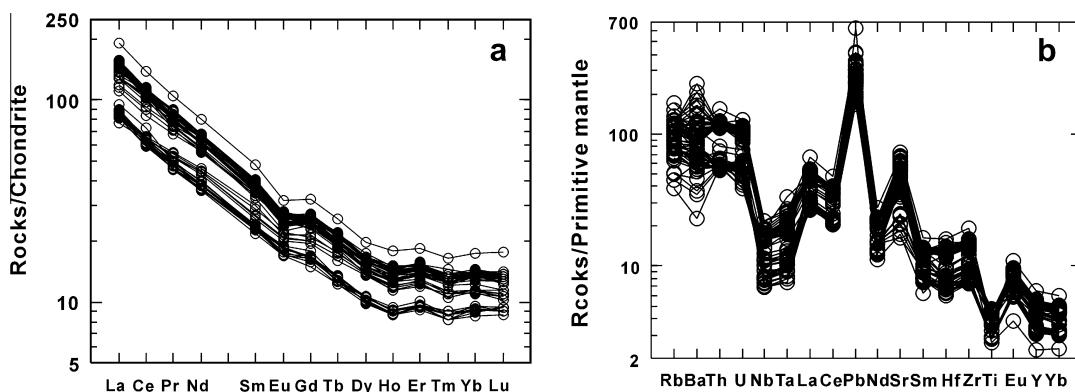
Fig. 5. Chondrite-normalized rare earth element patterns and primitive mantle-normalized spider diagrams of volcanic rocks from the Gerze area, southern Qiangtang Terrane, China. Primitive mantle and chondritic abundances were taken from Sun and McDonough (1989).
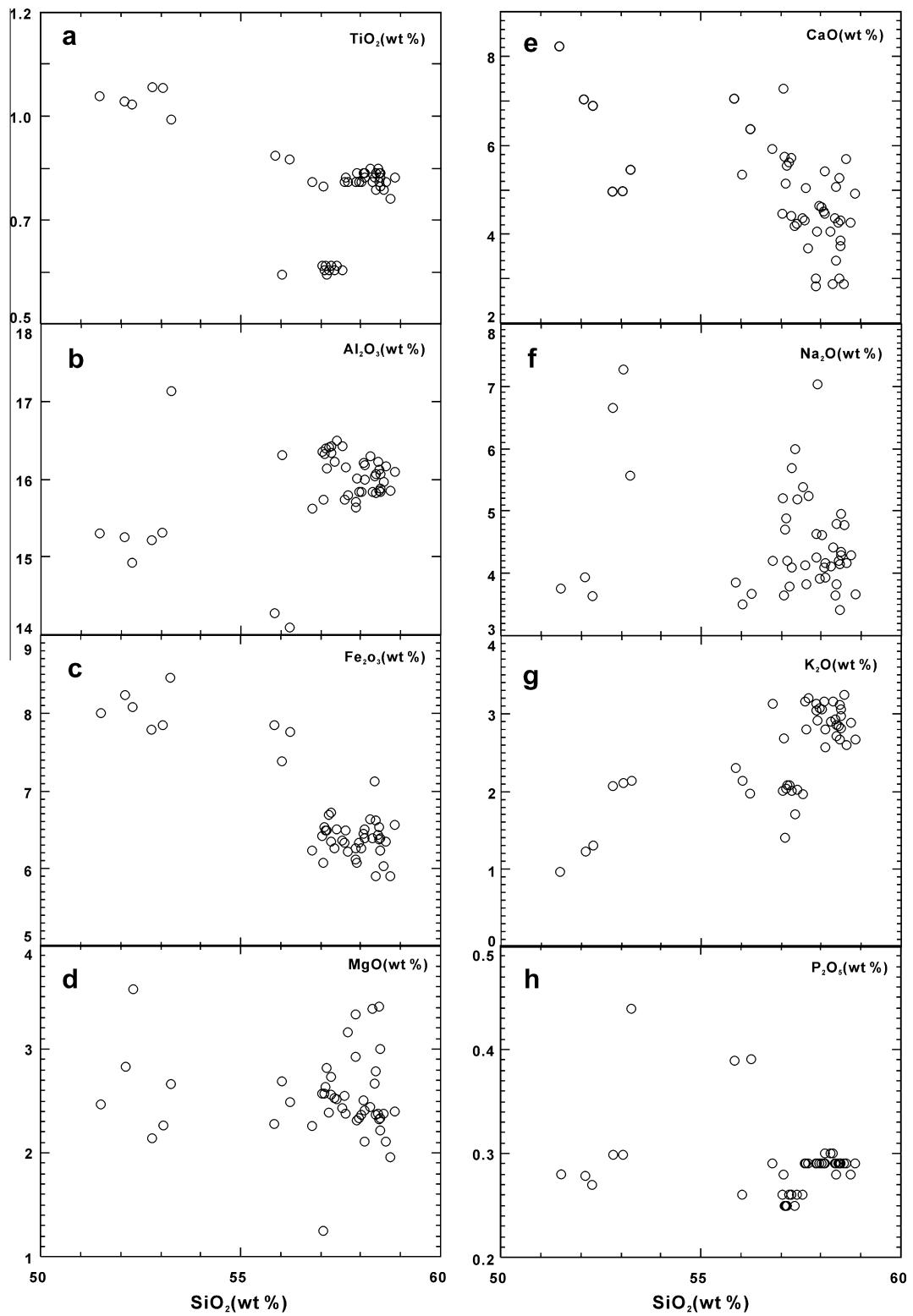
Fig. 6. SiO$_2$ versus TiO$_2$, Al$_2$O$_3$, Fe$_2$O$_3$, MgO, CaO, Na$_2$O, K$_2$O, and P$_2$O$_5$ for volcanic rocks from the Gerze area, southern Qiangtang Terrane, China.

of crustal contamination (Fig. 9a and b). The studied andesites are further characterized by relatively low contents of Nb (4.95–15.5 ppm), Zr (84–180 ppm), Th (4.48–13.1 ppm), and Rb (24.7–80.9 ppm) compared to the upper crust (which yields typical values of Nb = 25 ppm, Zr = 190 ppm, Th = 10.5 ppm, and Rb = 84 ppm; Rudnick and Fountain, 1995; Rudnick and Gao, 2003), again suggesting negligible crustal contamination. The

degree of crustal contamination can be also assessed from (Th/Yb)$_{PM}$ ratios, where the rock values are normalized to the relevant trace-element contents of primitive mantle (Qi and Zhou, 2008). In addition, the andesites are characterized by relatively lower Nb (4.89–15.5 ppm) and U (0.81–2.69 ppm) compared with the upper crust (e.g., Nb = 25 ppm, U = 2.7 ppm, Rudnick and Fountain, 1995; Rudnick and Gao, 2003), suggesting that crustal contamination was
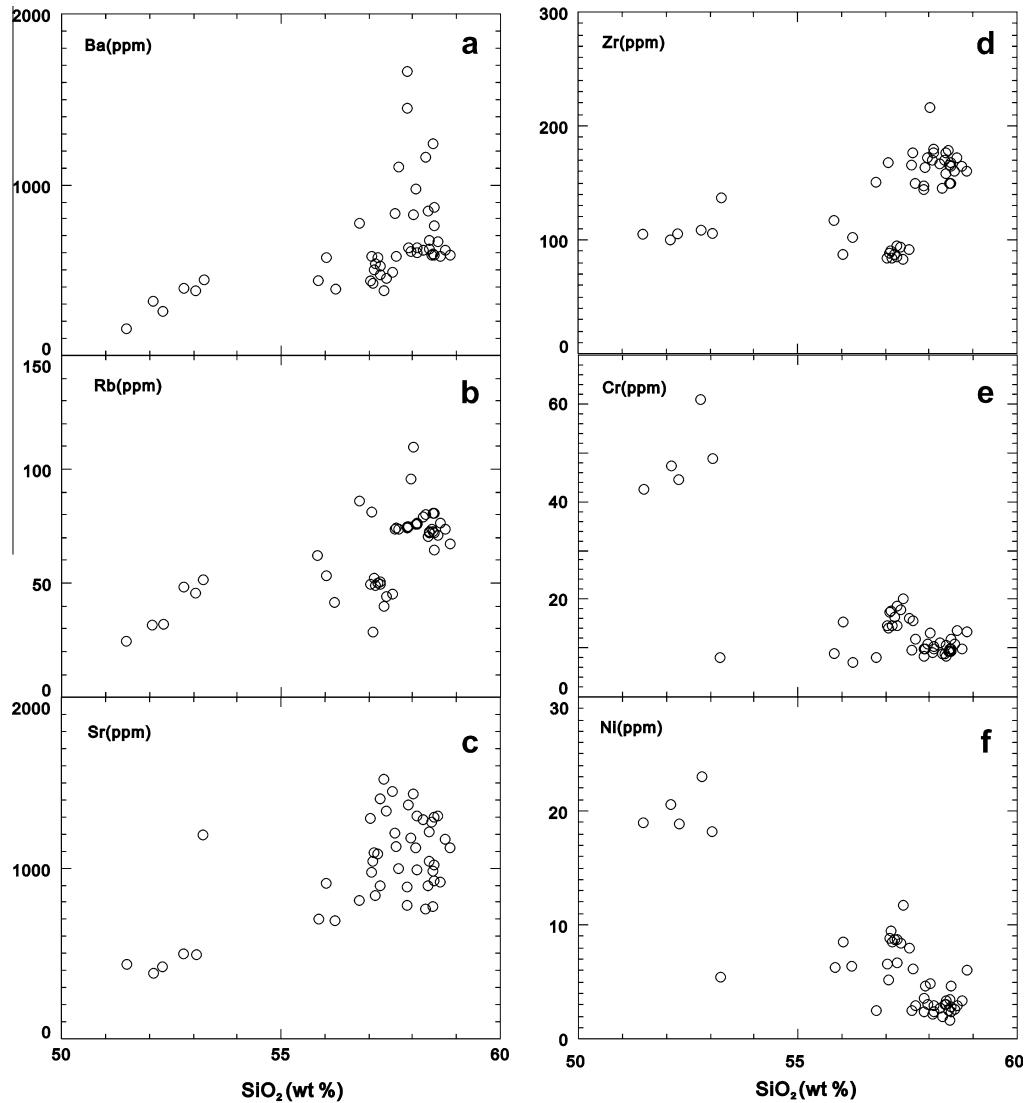
Fig. 7. SiO_2 versus Ba, Rb, Sr, Zr, Cr, and Ni for volcanic rocks from the Gerze area, southern Qiangtang Terrane, China.
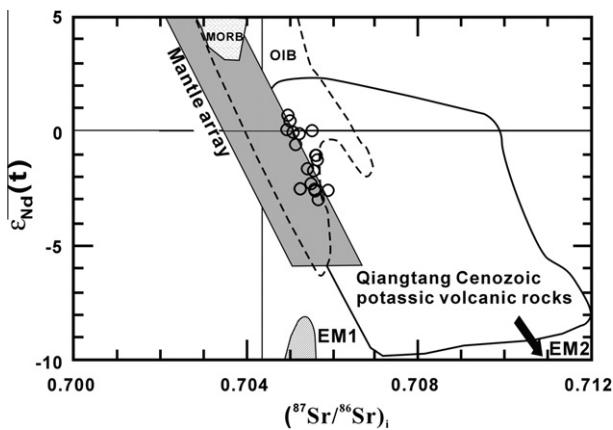
Fig. 8. $(^{87}Sr/^{86}Sr)_i$ versus $\varepsilon_{Nd}(t)$ for volcanic rocks from the Gerze area, southern Qiangtang Terrane, China.

insignificant in these rocks. The lack of correlation between the $\varepsilon_{Nd}(t)$ values and Nd concentrations for the andesites (not presented) precludes assimilation and fractional crystallization (AFC)

as a major process during their late evolutionary stages, at a shallow crustal level. Otherwise, samples of the Gerze volcanic rocks have much lower $(Th/Yb)_{PM}$ ratios (14.2–26.8) than those of the upper crust (28; Taylor and Mclennan, 1985), consistent with negligible crustal contamination. In summary, we conclude that the geochemical and Sr–Nd isotopic signatures of the Gerze volcanic rocks are inherited mainly from the source prior to emplacement and do not reflect significant crustal assimilation.

5.2. Fractional crystallization

For the studied andesite samples, SiO_2 shows a negative correlation with TiO_2, Al_2O_3, Fe_2O_3, MgO, CaO, Na_2O, P_2O_5 (Fig. 6a–f, h), and Zr (Fig. 7d), probably related to the fractionation of clinopyroxene, hornblende, plagioclase, Ti-bearing phases (rutile, ilmenite, titanite, etc.), apatite, and zircon. The negative Ti anomalies in all the rocks (Fig. 6b) also agree with the fractionation of Fe–Ti oxides such as rutile and ilmenite. In addition, most of the samples show slightly negative Ba anomalies (Fig. 6a), indicating the fractionation of K-feldspar. The positive correlations between MgO and each of Fe_2O_3 and CaO (data not shown) indicate that the volcanic rocks are likely generated by the olivine-, pyroxene-, and hornblende-dominated fractionation from a parent basaltic magma.
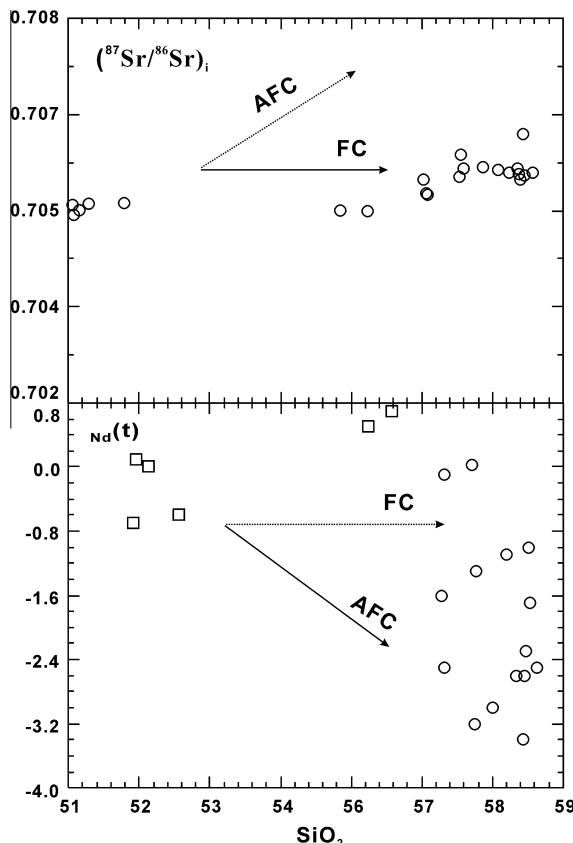
Fig. 9. Plots of the (a) initial $^{87}Sr/^{86}Sr$ ratio and (b) $\varepsilon_{Nd}(t)$ versus MgO for volcanic rocks from the Gerze area, southern Qiangtang Terrane, China, indicating crystal fractionation. FC: fractional crystallization; AFC: assimilation and fractional crystallization.

The negative correlation between MgO and Al_2O_3 (data not shown) suggests that plagioclase is not a major fractionating phase for the andesites, which is further supported by the lack of negative Sr anomalies and absence of strongly negative Eu anomalies (Fig. 5).

The general finding of negative Nb, Ta, and Ti anomalies in the analyzed samples (Fig. 5b) supports the fractionation of Fe–Ti oxides (e.g., rutile, ilmenite, and titanite) or that these magmas formed in a destructive-margin environment with a residual Ti-bearing phase (e.g., spinel) in the mantle source during partial melting.

The andesites show a decrease of Zr with increasing SiO_2 (Fig. 7d), indicating that zircon was saturated in the magma and was also a major fractionating phase (Li et al., 2007). Zircon saturation thermometry (Watson and Harrison, 1983) provides a simple and robust means of estimating the temperature of felsic magma from bulk-rock compositions. The calculated zircon saturation temperatures (TZr°C) of the andesite samples range from 729 to 824 °C (Table 3), which is most likely a minimum temperature of formation.

5.3. Genetic model

Three genetic models have been proposed to generate intermediate volcanic rocks: (1) fractional crystallization from basaltic magma, because andesite usually accretes with basalt and these rocks have similar Sr isotopic compositions; (2) combined magma assimilation and AFC; and (3) partial melting of crustal rocks at depth, possibly as a result of underplating (Zhu et al., 2006). Hence, we now try to discover how the studied volcanic rocks were

formed. The geochemical and isotopic evidence presented above shows that the data do not support crustal involvement; thus, we can exclude the second model. Consequently, we examine the possibility that the andesites were derived by the first or the third model.

The third model is widely accepted for the generation of magmas, including primary andesites, at destructive plate margins (e.g., Hawkesworth et al., 1994). Above all, this model should be supposed by melting of the downgoing slab or underplated (crustal) basalt; however, this model is not supported by the data of this paper. The andesites are not produced through crustal melting; thus, this model is not a likely mode to form Gerze volcanic rocks.

Based on the analysis above, we need to discuss the possibility of the first model. The data indicate that the geochemical and isotopic signature of the andesites reflects that of heterogeneous mantle source. In addition, there is evidence that the andesites have experienced some degree of fractional crystallization, that is, they were derived from parental magmas more mafic than andesites (basalts or "primitive or primary" andesites). The fact that there are no basalt in the study area, however, indicates that fractional crystallization of the basalts could have occurred at depth (i.e., the basalts could have been underplated). Thus, the parental basalts are still at depth. Alternatively, the basalts could have been eroded already. On the basis of the discussion above, we now prefer to study volcanic rocks that were derived from the first model; that is, as fractional crystallization from basaltic magma.

6. Conclusions

Using geochronological, geochemical, and Sr–Nd isotopic data as bases, we draw the following conclusions concerning the origins of the Gerze andesites. These are summarized as follows.

(1) LA–ICP–MS U–Pb zircon age data indicate that the andesites were formed between 122.4 ± 0.4 Ma and 124.4 ± 0.4 Ma.
(2) The andesites belong to the alkaline and sub-alkaline magma series, and show both calc-alkaline and high-K calc-alkaline affinities as indicated by their K_2O and Na_2O contents. The rocks are enriched in light rare earth elements [$(La/Yb)_N$ = 7.4–11.5)] and large-ion lithophile elements (e.g., Rb), and show slightly negative Eu anomalies (Eu/Eu* = 0.79–0.94) and negative anomalies in high field strength elements (Nb, Ta, and Ti) relative to primitive mantle. These geochemical features are typical of magmas formed in a destructive plate-margin setting.
(3) The andesites were derived from a compositionally heterogeneous mantle source. The parent magmas probably originated via fractional crystallization from a basaltic magma (was underplated or eroded). Fractionation (involving olivine, pyroxene, hornblende, and to a lesser extent, plagioclase) occurred during ascent of the andesite, with negligible crustal contamination.

References

Allègre, C.J., Courtillot, V., Tapponnier, P., Hirn, A., Mattauer, M., Coulon, C., Jaeger, J.J., Achache, J., Schärer, U., Marcoux, J., Burg, J.P., Girardeau, J., Gariépy, C., Gopel, C., Li, T.D., Xiao, X.C., Chang, C.F., Li, G.G., Lin, B.Y., Teng, J.W., Wang, N.W., Chen, G.M., Han, T.L., Wang, X.B., Sheng, H.B., Cao, Y.Q., Zhou, J., Giu, H.R., Bao, P.S., Wang, S.C., Wang, B.X., Zhou, Y.X., Ronghua, X., 1984. Structure and evolution of the Himalaya-Tibet orogenic belt. Nature 307, 17–22.

Andersen, T., 2002. Correction of common lead in U–Pb analyses that do not report [204]Pb. Chemical Geology 192, 59–79.

Bai, Y.S., Li, L., Niu, Z.J., Cui, J.L., 2005. Characteristics and Tectonic Setting of Eerlongba Formation Volcanic Rocks in Geladandong Area of Central Qiangtang. Acta Geoscientica Sinica 26, 113–120.

Chang, C.F., Chen, N.S., Coward, M.P., Deng, W.M., Dewey, J.F., Gansser, A., Narris, N.B.W., Jin, C.W., Kidd, W.S.F., Leeder, M.R., Li, H., Lin, J.L., Liu, C.J., Mei, H.J., Molnar, P., Pan, Y., Pan, Y.S., Pearce, J.A., Shackleton, R.M., Smith, A.B., Sun, Y.Y., Ward, M., Watts, D.R., Xu, J.T., Xu, R.H., Yin, J.X., Zhang, Y.Q., 1986. Preliminary conclusions of the Royal society/Aeademia Siniea 1985 Geotraverse of Tibet. Nature 323, 501–507.

Chi, X.G., Li, C., Jin, W., 2005. Cenozoic volcanism and tectonic evolution of lithosphere in Qiangtang, northern Tibet. Science in China 35, 399–401.

Chung, S.L., Zhang, Y.Q., Xie, Y.W., Lo, C.H., Chu, M.F., Lee, T.Y., Li, X.H., Zhang, Q., Wang, Y.Z., 2005. Tibetan tectonic evolution inferred from spatial and temporal variations in Post-collisional magmatism. Earth-Science Reviews 68, 173–196.

Deng, W.M., 1989. The Cenozoic volcanic in north Ali area, Xizang. Acta Petrologica Sinica 3, 1–11 (in Chinese with English abstract).

Deng, W.M., 1998. Cenozoic intraplate volcanic rocks in the northern Qinghai-Xizang plateau. Geological Publishing House, Beijing, 1–178.

Deng, W.M., 1999. The geology, geochemistry and forming age of the shoshonitic volcanic rocks in middle Kunlun orogenic belt. Scientia Geologica Sinica 3, 201–213 (in Chinese with English abstract).

Dewey, J.F., Shackleton, R.M., Chang, C., Sun, Y.Y., 1988. The tectonic development of the Tibet plateau. Philosophical Transactions of the Royal Society of London, Series A 327, 379–413.

Ding, L., Zhang, J.J., Zhou, Y., Deng, W.M., Xu, R.H., Zhong, D.L., 1999. Tectonic implication on the lithosphere evolution of the Tibet plateau: petrology and northern Tibet. Acta Petrogica Sinica 15, 408–421.

Ding, L., Kapp, P., Zhong, D., Deng, W., 2003. Cenozoic volcanism in Tibet: evidence for a transition from oceanic to continental subduction. Journal of Petrology 44, 1833–1865.

Ding, L., Kapp, P., Yue, Y.H., Lai, Q.Z., 2007. Post collisional calc-alkaline lavas and xenoliths from the southern Qiangtang Terrane, central Tibet. Earth and Planetary Science Letters 255, 28–38.

Girardeau, J., Marcoux, J., Bassoullet, J.P., Tang, Y.K., Xiao, X.C., Zao, Y.G., Wang, X.B., 1984. Tectonic environment and geodynamic significance of the Neo-Cimmerian Dongqiao ophiolite, Bangong-Nujiang suture zone, Tibet. Nature 307, 27–31.

Girardeau, J., Marcoux, J., Fourcade, E., Bassoullet, J.P., Tang, Y.K., 1985. Xainxa ultramafic rocks, central Tibet, China: Tectonic environment and geodynamic significance. Geology 13, 330–333.

Guo, Z.F., Wilson, M., Liu, J.Q., Mao, Q.A., 2006. Post-collisional potassic and ultrapotassic magmatism of the northern Tibetan plateau: constraints on characteristics of the mantle source, geodynamic setting and uplift mechanisms. Journal of Petrology 47, 1177–1220.

Hawkesworth, C.J., Gallagher, K., Hergt, J.M., McDermott, F., 1994. Destructive plate margin magmatism: Geochemistry and melt generation. Lithos 33, 169–188.

Lai, S.C., Liu, C.Y., 2001. Enriched upper mantle and eclogitic lower crust in north Qiangtang, Qinghai–Tibet Plateau: petrological and geochemical evidence from the Cenozoic volcanic rocks. Acta Petrologica Sinica 17, 459–468 (in Chinese with English abstract).

Li, C., Huang, X.P., Mou, S.Y., Chi, X.G., 2006. [40]Ar–[39]Ar dating for Kangtog formation volcanic rocks in Zougouyouchaco, Qiangtang, northern Tibet. Geological Bulletin of China 25, 226–228 (in Chinese with English abstract).

Li, X.H., Li, Z.X., Li, W.X., Liu, Y., Yuan, C., Wei, G.J., Qi, C.S., 2007. U–Pb zircon, geochemical and Sr–Nd–Hf isotopic constraints on age and origin of Jurassic I- and A-type granites from central Guangdong, SE China: a major igneous event in response to foundering of a subducted flat-slab? Lithos 96, 186–204.

Liu, S., Hu, R.Z., Chi, X.G., Li, C., Feng, C.X., 2003. Geochemistry, series subdivision and petrogenetic interpretation of Cenozoic volcanic rocks in northern Tibet. Geological Journal of China University 9, 279–292.

Liu, S., Hu, R.Z., Feng, C.X., Zou, H.B., Chi, X.G., Peng, J.T., Zhong, H., Qi, L., Qi, Y.Q., Wang, T., 2008. Cenozoic high Sr/Y volcanic rocks in the Qiangtang Terrane, northern Tibet: geochemical and isotopic evidence for the origin of delaminated lower continental crust. Geologic Magazine 145, 463–474.

Ludwig, K.R., 2003. User's manual for Isoplot/Ex, Version 3.00. A Geochronological Toolkit for Microsoft Excel: Berkeley Geochronology Center Special Publication 4, 1–70.

Menzies, M.A., Pyle, P.R., 1990. Continental volcanism: A crust-mantle Probe. In: Menzies, M.A. (Ed.), Continental Mantle. Clarendon Press, Oxford, pp. 57–177.

Miller, C., Sehuster, R., Klotzli, U., Mair, V., Frank, W., Purtseheller, F., 1999. Postcollisional Potassic and ultraPotassic magmatism in SW Tibet: geochemical and Sr-Nd-Pb-0 isotopic constrains for mantle sources characteristics and petrogenesis. Journal of Petrology 40, 1399–1424.

Potts, P.J., Kane, J.S., 2005. International association of geoanalysts certificate of analysis: certified reference material OU-6 (Penrhyn slate). Geostandards and Geoanalytical Research 29, 233–236.

Qi, L., Zhou, M.F., 2008. Platinum-group elemental and Sr-Nd–Os isotopic geochemistry of Permian Emeishan flood basalts in Guizhou Province, SW China. Chemical Geology 248, 83–103.

Qi, L., Hu, J., Grégoire, D.C., 2000. Determination of trace elements in granites by inductively coupled plasma mass spectrometry. Talanta 51, 507–513.

Rudnick, R.L., Fountain, D.M., 1995. Nature and composition of the continental crust: a lower crustal perspective. Reviews of Geophysics 33, 267–309.

Rudnick, R.L., Gao, S., 2003. Composition of the continental crust. In: Rudnick, R.L. (Ed.), the Crust (vol. 3. Treatise on the Geochemistry. Edited by H.D. Holland and K.K. Turekian). Elsevier-Pergamon, Oxford, pp. 1–64.

Sun, S.S., McDonough, W.F., 1989. Chemical and isotopic systematics of o c e a n i c basalts: implications for mantle composition and processes. In: Saunders, A.D., Norry, M.J. (Eds.), Magmatism in the Ocean Basins. Geological Society Special Publication, London, pp. 313–345.

Taylor, S.R., McLennan, S.M., 1985. The continental crust: its composition and evolution. An Examination of the Geochemical Record Preserved in Sedimentary Rocks. Blackwell Scientific Publication, Oxford, pp. 46.

Thompson, M., Potts, P.J., Kane, J.S., Wilson, S., 2000. An International Proficiency Test for Analytical Geochemistry Laboratories-Report on Round 5 (August 1999). Geostandards and Geoanalytical Research 24, E1–E28.

Turner, S., Arnaud, N., Liu, J., Rogers, N., Hawkesworth, C., Harris, N., Kelley, S., van Calsteren, P., Deng, W., 1996. Post-collision, Shoshonitic volcanism on the Tibetan Plateau: Implications for Convective Thinning of the Lithosphere and the Source of Ocean Island Basalts. Journal of Petrology 37, 45–71.

Wang, Y.M., Gao, Y.S., Han, H.M., Wang, X.H., 2003. Practical Handbook of Reference Materials for Geoanalysis. Geological Publishing House (in Chinese).

Watson, E.B., Harrison, T.M., 1983. Zircon saturation revisited: temperature and composition effects in a variety of crustal magma types. Earth and Planetary Science Letters 64, 295–304.

Williams, H.M., Tumer, S.P., Pearce, J.A., Kelley, S.P., Harris, N.B.W., 2004. Nature of the source regions for Post-collisional, Potassic magmatism in southern and northern Tibet from geochemical variations and inverse trace element modeling. Journal of Petrology 45, 555–607.

Yin, A., Harrison, T.M., 2000. Geology evolution of the Himalayan-Tibetan Orogen. Annual Review of Earth and Planetary Science 28, 211–280.

Yin, H.S., Lin, J.H., Li, B.H., Zhao, B., Shi, Z.Q., Yuan, J.J., Sun, C.M., Lai, S.C., Zhu, Y.T., Zhao, X.X., 2004. Cenozoic high-K clca-alkaline series volcanic rocks and interaction of crust and mantle in northern Tibet Plateau. The Geological Publishing House (in Chinese) 1–95.

Yuan, H.L., Gao, S., Liu, X.M., Li, H.M., Gunther, D., Wu, F.Y., 2004. Accurate U–Pb age and trace element determinations of zircon by laser ablation-inductively coupled plasma mass spectrometry. Geostandards Newsletter 28, 353–370.

Zhu, D.C., Pan, G.T., Mo, X.X., Wang, L.Q., Zhao, Z.D., Geng, Q.R., 2006. Identification for the Mesozoic OIB-type Basalts in Central Qinghai-Tibetan Plateau: Geochronology, Geochemistry and Their Tectonic Setting. Acta Geologica Sinica 80, 1312–1328.